Biophysical *Journal*
Biophysical Letter

Biophysical Society

Quantifying Instrumental Artifacts in Folding Kinetics Measured by Single-Molecule Force Spectroscopy

Krishna Neupane[1] and Michael T. Woodside[1,2,*]
[1]Department of Physics, University of Alberta, Edmonton, Alberta, Canada; and [2]National Institute for Nanotechnology, National Research Council, Edmonton, Alberta, Canada

ABSTRACT Force spectroscopy is commonly used to measure the kinetics of processes occurring in single biological molecules. These measurements involve attaching the molecule of interest to micron-sized or larger force probes via compliant linkers. Recent theoretical work has described how the properties of the probes and linkers can alter the observed kinetics from the intrinsic behavior of the molecule in isolation. We applied this theory to estimate the errors in measurements of folding made using optical tweezers. Errors in the folding rates arising from instrument artifacts were only ~20% for constant-force measurements of DNA hairpins with typical choices of linker length and probe size. Measurements of transition paths using a constant trap position at high trap stiffness were also found to be in the low-artifact limit. These results indicate that typical optical trap measurements of kinetics reflect the dynamics of the molecule fairly well, and suggest practical limitations on experimental design to ensure reliable kinetic measurements.

Single-molecule force spectroscopy (SMFS), in which tension is applied to individual molecules via mechanical probes (1), has been used widely to study the properties of macromolecules, in particular the conformational dynamics of proteins and nucleic acids (2). SMFS measurements involve force probes like atomic force microscopes or optical or magnetic tweezers that apply load to the molecule being studied via mechanical linkers connecting the molecule to the probe (Fig. 1 A, *upper inset*). Because only the probe motion is observed directly, not the motion of the molecule itself, the properties of the latter must be inferred from the former. The probe and linker dynamics may then alter the observed response from the intrinsic molecular behavior that would have been expected without this coupling, complicating the interpretation of data.

Analysis of SMFS experiments has often assumed that the effects of the instrumental coupling can be ignored, as in the classic Bell-Evans-Zhurkov model for the force-dependent kinetics of folding and unfolding (3). However, experimental and theoretical studies of the ways that SMFS assay implementation can alter observations have provided improved frameworks for more reliable analysis of SMFS data (4–12). A particularly important focus has been on the effects of the probe size and linker stiffness (12–18), with recent work showing how these can alter the apparent values of properties like the conformational diffusion coefficient (15–17) or the kinetics (18). Here, we apply the framework of Cossio et al. (18) to gauge the extent to which the rates and transition path times observed in SMFS folding studies are distorted by instrumental effects under typical experimental conditions, using DNA hairpins measured in optical tweezers (19) as a model system.

DNA hairpins of specific sequences that fold as two-state systems were connected at each end to polystyrene beads (820- and 600-nm diameter) via double-stranded DNA linkers of total length ~2000 basepairs, as described previously in Woodside et al. (19). Two kinetic properties were investigated: 1) the folding rates, measured in equilibrium at a constant force maintained by a passive force clamp (20) to avoid feedback-loop artifacts (9), with the stiffness of the two traps set at 0.3 and 0 pN/nm; and 2) the transition path times, i.e., the time required to move across the energy barrier between the two states, measured in equilibrium at a constant trap position using stiff traps (0.56–0.63 and 0.75–1.1 pN/nm). In both cases, the force was kept near the value, $F_{1/2}$, where the hairpins occupied the folded (F) and unfolded (U) states with equal probability.

The folding rates measured from extension trajectories at constant force (Fig. 1 A), denoted k_{MA}, are listed in Table 1.

Submitted January 20, 2016, and accepted for publication June 14, 2016.
*Correspondence: michael.woodside@ualberta.ca
Editor: Thomas Perkins.
http://dx.doi.org/10.1016/j.bpj.2016.06.011

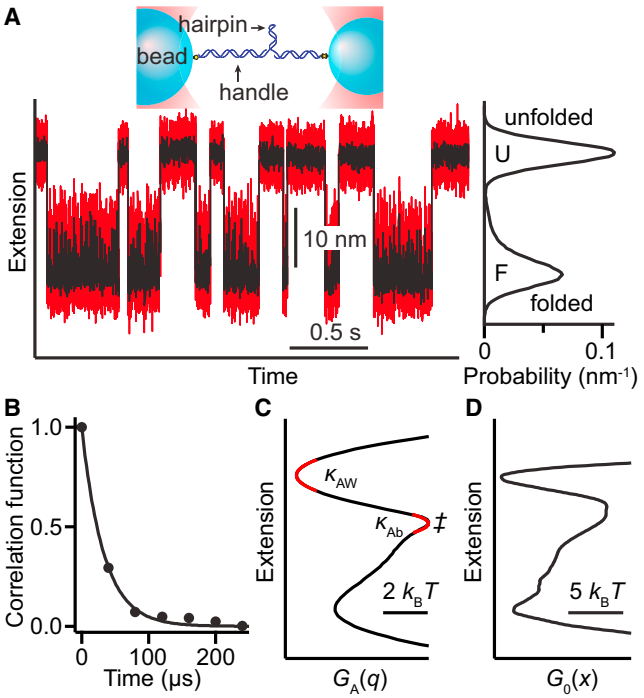

FIGURE 1 **Analysis of rates. (*A*) Extension trajectory for hairpin 30R50/T4 at constant force. (*Upper inset*) Schematic of measurement showing hairpin attached to beads via DNA handles. (*Right inset*) Probability density from trajectory. (*B*) Decay of extension autocorrelation in unfolded state yields τ_A. (*C*) PMF from the extension trajectory, yielding κ_{Ab}, κ_{Aw}, and $\Delta G_A^{\ddagger}$. (*D*) Landscape obtained by deconvolution of PMF. To see this figure in color, go online.**

To determine how well these rates reflect the true folding rates, denoted k_M, we first estimated the rate k_A expected if the system were diffusing over the potential of mean force (PMF) along the measured extension coordinate, $G_A(q)$, with the diffusion coefficient implied by the extension dynamics observed, D_q (18). Only if k_A is fast compared to k_{MA} can the latter be a good estimate of k_M (18). D_q reflects the contributions from the beads and linkers, and is defined by $D_q = \langle \delta q^2 \rangle / \tau_A$, where δq is the deviation of extension from its average value within F or U and τ_A the relaxation time obtained via single-exponential fits of the extension autocorrelation function within the same state (Fig. 1 B). D_q, listed in Table 1, was the same for both F and U (Table S1 in the Supporting Material); notably, it was a bit slower than the free diffusion of a bead alone (7×10^5 nm^2/s). We then used $G_A(q)$ (Fig. 1 C), found from the logarithm of the extension probability distribution (Fig. 1 A, *right inset*), to obtain k_A via Kramers' equation:

$$k_A = {}^1/_{2\pi} \sqrt{\kappa_{Ab}\kappa_{Aw}}\beta D_q \exp\left(-\beta \Delta G_A^{\ddagger}\right), \qquad (1)$$

where $\Delta G_A^{\ddagger}$ is the barrier height in the PMF, κ_{Ab} is the barrier stiffness, κ_{Aw} is the well stiffness, and β is the inverse thermal energy. The results for hairpins 30R50/T4 and 20TS06/T4 from Woodside et al. (4) are listed in Tables 1 and S1.

TABLE 1 **Kinetic Parameters, Average of Folded and Unfolded**

	30R50/T4	20TS06/T4
Constant Force		
D_q ($\times 10^5$ nm^2/s)	2.4 ± 0.2	4.0 ± 0.3
k_A (s^{-1})	105 ± 7	700 ± 100
k_{MA} (s^{-1})	3.3 ± 0.2	11 ± 3
k_M (s^{-1})	4 ± 1	15 ± 3
D_x ($\times 10^5$ nm^2/s) (via Kramers')	4.6 ± 0.5	5 ± 3
Constant Trap Position		
D_q ($\times 10^5$ nm^2/s)	6.0 ± 0.3	5.7 ± 0.3
D_x ($\times 10^5$ nm^2/s) (transition time)	4.4 ± 0.4	3.4 ± 0.8

Comparing k_A and k_{MA} (Table 1), we found that indeed $k_A \gg k_{MA}$. Thus $k_{MA} \approx k_M$, and the error caused by instrumental effects could be estimated from (18)

$$[k_{MA}]^{-1} = \left[k_M\left(1 - \left[\beta|\kappa_b|\left\langle \delta q^2 \right\rangle\right]^{-1}\right)\right]^{-1} + [k_A]^{-1}, \qquad (2)$$

where κ_b is the barrier stiffness in $G_0(x)$ (Fig. 1 D), the intrinsic energy landscape, found by deconvolving the effects of instrument compliance (4,21). From Eq. 2, k_{MA} was 20–30% lower than k_M (Table 1). The rate artifacts were thus small, similar in size to the experimental uncertainty in the rates. As $(\beta\langle\delta q^2\rangle)^{-1}$ varies with the system stiffness, small errors require the system stiffness to be less than the barrier stiffness. The errors were not force-dependent: repeating the analysis of hairpin 20TS06/T4 at a force where it was 99.7% unfolded and the rates for folding and unfolding differed greatly (respectively, $k_{MA} = 1.4$ and 290 s^{-1} (Table S2)), we found $k_M = 1.5$ and 330 s^{-1}, respectively—indicating an error of ~10–15%, similar to that near $F_{1/2}$.

Turning next to the effects of the instrument on transition-path time measurements, we note that these are expected to be small when $D_q \gtrsim D_x$, the diffusion coefficient along the intrinsic molecular free-energy profile (18). Transition path times have recently been measured directly with SMFS for the first time (22,23). Measuring the same hairpins but now at constant trap position (Fig. 2 A), we recalculated D_q as above from the extension fluctuations and autocorrelation function (Fig. 2 B). D_q was noticeably faster than in constant-force measurements (Table 1), because the higher trap stiffness decreased τ_A more than it did $\langle \delta q^2 \rangle$ (which depends on the well stiffness as well as the trap stiffness). D_x was found in two ways: from the constant-force kinetics, via Kramers' equation applied to the energy profile obtained after instrument compliance effects on $G_A(q)$ (Fig. 2 C) were removed by deconvolution (15,21); and from the average transition-path time measured from constant-position trajectories (23) using Eq. S1 (Table S1). The two methods yielded the same result. For both hairpins, $D_x < D_q$ in these measurements (Table 1), suggesting that the

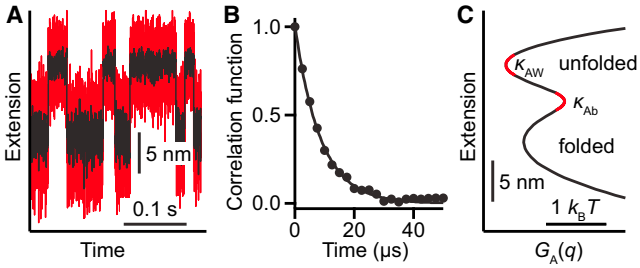

FIGURE 2 Constant trap position measurements. (*A*) Extension trajectory for hairpin 20TS06/T4. (*B*) Decay of extension autocorrelation in unfolded state yields τ_A. (*C*) PMF from extension trajectory yields κ_{Ab}, κ_{Aw}, and $\Delta G_A^{\ddagger}$. To see this figure in color, go online.

observed transition paths should not be distorted too much by instrumental artifacts.

This work shows that for typical optical trapping assays, using 1/2–1 μm beads and 1–2 kb double-stranded DNA linkers, the rates observed are predicted to be close to the intrinsic molecular rates. Only minor artifacts arise from the linkers and beads, giving confidence that the observed behavior reflects the molecular dynamics faithfully. The 20–30% error predicted by the theory matches well with the error found empirically in previous work by Chang et al. (14). Large bead-size or linker-stiffness increases may lead to larger artifacts, however, as noted previously (15–18); this is unfortunate because stiff linkers in particular allow for easier reconstruction of free-energy profiles (10,11,24,25). Optimizing assay design for one purpose (e.g., landscape reconstruction) may thus degrade its suitability for others (e.g., measuring kinetic properties). Furthermore, molecules with very soft barriers (low κ_b) are especially susceptible to artifacts (17,18) and may thus require special attention to linker design. As it turns out, however, ~2 kb DNA linkers represent a decent compromise, allowing both reliable kinetic measurements and landscape reconstructions even for molecules with relatively soft barriers like DNA hairpins.

We can estimate the errors expected if stiffness or bead size is increased up to or beyond the practical limits for optical tweezers measurements by considering the effects on hairpin 30R50/T4. Because bead size primarily affects τ_A (increasing τ_A roughly linearly with bead size in the large bead limit), changing $\langle \delta q^2 \rangle$ and $G_A(q)$ little, using 10-fold larger beads would decrease k_A ~10-fold, roughly doubling the rate error from Eq. 2. Larger effects are seen from stiffness changes: if the system stiffness values were high enough to avoid the need for compliance deconvolution (higher than the stiffness of any feature in the landscape), then assuming only order-unity changes in D_q (because both τ_A and $\langle \delta q^2 \rangle$ would be smaller), k_A would be reduced ~100-fold, because $\Delta G_A^{\ddagger}$ would increase from ~4 to 9 k_BT (15), leading to $k_A \approx k_{MA}$ rather than $k_A \gg k_{MA}$ as above.

These examples suggest how rate artifacts may manifest in other SMFS assays. Magnetic tweezers assays usually use DNA linkers like those above, so slow τ_A arising from large bead size (usually ~2–10 μm) is likely to be the main source of artifacts. Atomic force microscope assays are often done using short peptide linkers and much stiffer force probes (cantilevers); artifacts may thus arise primarily from reductions in k_A so that $k_A \approx k_{MA}$. Shaping the cantilever to optimize stiffness, drag, and time response (26) may help reduce its contribution to errors, but artifacts will also arise from the significant compliance difference when varying numbers of repeats are unfolded in the tandem-repeat constructs most often used (18). Single-repeat constructs with longer, more compliant linkers may then be needed for accurate rate measurements. Finally, other artifacts not considered here, such as basculation effects in traps (27) and feedback-loop artifacts (9,12), can also alter the observed rates.

SUPPORTING MATERIAL

Supporting Materials and Methods and two tables are available at http://www.biophysj.org/biophysj/supplemental/S0006-3495(16)30449-0.

AUTHOR CONTRIBUTIONS

K.N. and M.T.W. designed research and wrote the article, and K.N. performed research.

ACKNOWLEDGMENTS

We thank A. Szabo for helpful discussions.

This work was supported by Alberta Innovates Technology Futures and Natural Sciences and Engineering Research Council Canada.

REFERENCES

1. Neuman, K. C., and A. Nagy. 2008. Single-molecule force spectroscopy: optical tweezers, magnetic tweezers and atomic force microscopy. *Nat. Methods.* 5:491–505.
2. Ritchie, D. B., and M. T. Woodside. 2015. Probing the structural dynamics of proteins and nucleic acids with optical tweezers. *Curr. Opin. Struct. Biol.* 34:43–51.
3. Evans, E., and K. Ritchie. 1997. Dynamic strength of molecular adhesion bonds. *Biophys. J.* 72:1541–1555.
4. Woodside, M. T., P. C. Anthony, …, S. M. Block. 2006. Direct measurement of the full, sequence-dependent folding landscape of a nucleic acid. *Science.* 314:1001–1004.
5. Dudko, O. K., G. Hummer, and A. Szabo. 2008. Theory, analysis, and interpretation of single-molecule force spectroscopy experiments. *Proc. Natl. Acad. Sci. USA.* 105:15755–15760.
6. Hyeon, C., G. Morrison, and D. Thirumalai. 2008. Force-dependent hopping rates of RNA hairpins can be estimated from accurate measurement of the folding landscapes. *Proc. Natl. Acad. Sci. USA.* 105:9604–9609.
7. Hinczewski, M., Y. von Hansen, and R. R. Netz. 2010. Deconvolution of dynamic mechanical networks. *Proc. Natl. Acad. Sci. USA.* 107:21493–21498.

8. Maitra, A., and G. Arya. 2011. Influence of pulling handles and device stiffness in single-molecule force spectroscopy. *Phys. Chem. Chem. Phys.* 13:1836–1842.
9. Elms, P. J., J. D. Chodera, …, S. Marqusee. 2012. Limitations of constant-force-feedback experiments. *Biophys. J.* 103:1490–1499.
10. Hinczewski, M., J. C. M. Gebhardt, …, D. Thirumalai. 2013. From mechanical folding trajectories to intrinsic energy landscapes of biopolymers. *Proc. Natl. Acad. Sci. USA.* 110:4500–4505.
11. Woodside, M. T., and S. M. Block. 2014. Reconstructing folding energy landscapes by single-molecule force spectroscopy. *Annu. Rev. Biophys.* 43:19–39.
12. Manosas, M., J.-D. Wen, …, F. Ritort. 2007. Force unfolding kinetics of RNA using optical tweezers. II. Modeling experiments. *Biophys. J.* 92:3010–3021.
13. Forns, N., S. de Lorenzo, …, F. Ritort. 2011. Improving signal/noise resolution in single-molecule experiments using molecular constructs with short handles. *Biophys. J.* 100:1765–1774.
14. Chang, J.-C., M. de Messieres, and A. La Porta. 2013. Effect of handle length and microsphere size on transition kinetics in single-molecule experiments. *Phys. Rev. E Stat. Nonlin. Soft Matter Phys.* 87:012721.
15. Woodside, M. T., J. Lambert, and K. S. D. Beach. 2014. Determining intrachain diffusion coefficients for biopolymer dynamics from single-molecule force spectroscopy measurements. *Biophys. J.* 107:1647–1653.
16. Makarov, D. E. 2014. Communication: Does force spectroscopy of biomolecules probe their intrinsic dynamic properties? *J. Chem. Phys.* 141:241103.
17. Nam, G.-M., and D. E. Makarov. 2016. Extracting intrinsic dynamic parameters of biomolecular folding from single-molecule force spectroscopy experiments. *Protein Sci.* 25:123–134.
18. Cossio, P., G. Hummer, and A. Szabo. 2015. On artifacts in single-molecule force spectroscopy. *Proc. Natl. Acad. Sci. USA.* 112:14248–14253.
19. Woodside, M. T., W. M. Behnke-Parks, …, S. M. Block. 2006. Nanomechanical measurements of the sequence-dependent folding landscapes of single nucleic acid hairpins. *Proc. Natl. Acad. Sci. USA.* 103:6190–6195.
20. Greenleaf, W. J., M. T. Woodside, …, S. M. Block. 2005. Passive all-optical force clamp for high-resolution laser trapping. *Phys. Rev. Lett.* 95:208102.
21. Neupane, K., D. B. Ritchie, …, M. T. Woodside. 2012. Transition path times for nucleic acid folding determined from energy-landscape analysis of single-molecule trajectories. *Phys. Rev. Lett.* 109:068102.
22. Yu, H., D. R. Dee, …, M. T. Woodside. 2015. Protein misfolding occurs by slow diffusion across multiple barriers in a rough energy landscape. *Proc. Natl. Acad. Sci. USA.* 112:8308–8313.
23. Neupane, K., D. A. N. Foster, …, M. T. Woodside. 2016. Direct observation of transition paths during the folding of proteins and nucleic acids. *Science.* 352:239–242.
24. Engel, M. C., D. B. Ritchie, …, M. T. Woodside. 2014. Reconstructing folding energy landscape profiles from nonequilibrium pulling curves with an inverse Weierstrass integral transform. *Phys. Rev. Lett.* 113:238104.
25. Pfitzner, E., C. Wachauf, …, H. Dietz. 2013. Rigid DNA beams for high-resolution single-molecule mechanics. *Angew. Chem. Int. Ed. Engl.* 52:7766–7771.
26. Edwards, D. T., J. K. Faulk, …, T. T. Perkins. 2015. Optimizing 1-μs-resolution single-molecule force spectroscopy on a commercial atomic force microscope. *Nano Lett.* 15:7091–7098.
27. Ribezzi-Crivellari, M., A. Alemany, and F. Ritort. 2015. Universal axial fluctuations in optical tweezers. *Opt. Lett.* 40:800–803.

Biophysical Journal, Volume *111*

Supplemental Information

Quantifying Instrumental Artifacts in Folding Kinetics Measured by Single-Molecule Force Spectroscopy

Krishna Neupane and Michael T. Woodside

Materials and Methods

Sample preparation: DNA hairpins attached to double-stranded (ds) DNA handles were prepared as described previously (1). Briefly, the hairpin was included as a 5′ overhang separated from a PCR priming sequence by abasic sites; the hairpin and 3′ handle (~800 bp long) were then made as a unit by PCR. A second handle (~1200 bp) made by PCR was then ligated to the 5′ end of the hairpin via complementary 5′ ligation sites. The hairpin-handle construct was attached to 600- and 820-nm polystyrene beads via biotin-avidin and dioxigenin and anti-dig pairs to generate bead-sample dumbbells for trapping. Hairpin samples were incubated for ~ 1 hr at ~ 100 pM with 250 pM polystyrene beads to form dumbbells. Dumbbells were diluted to ~ 500 fM in 50 mM MOPS, pH 7.5, with 200 mM KCl and oxygen scavenging system (8 mU/μL glucose oxidase, 20 mU/μL catalase, 0.01% w/v D-glucose), before insertion into a sample cell for optical trapping.

Measurements: All samples were measured on a dual-trap optical tweezers apparatus described previously (2). Briefly, two independently controlled traps were generated from a 4-W, 1064-nm, diode-pumped solid-state laser, splitting the traps by polarization. The stiffness and position of each trap were controlled respectively by acousto-optic and electro-optic deflectors. For constant force measurements, the stiffness of one trap was set to 0.3 pN/nm, whereas the other was used in the anharmonic region of the trap where the stiffness was zero, to achieve a passive force clamp (3). In constant trap position measurements, the stiffness set to 0.56–0.63 pN/nm in one trap and 0.75–1.1 pN/nm in the other; the effective system stiffness was thus several-fold higher in constant-position measurements, leading to a faster instrument response time (reflected in τ_A). Bead positions were detected by scattering a 7-mW, 633-nm HeNe laser off the beads and collecting the scattered light on position-sensitive detectors. Data were sampled at 20–256 kHz for constant-force measurements and 124–400 kHz for constant-position measurements, in each case filtered online at the Nyquist frequency.

Analysis: Rates were determined by thresholding analysis of the extension trajectories as described previously (1). The stiffness of the wells and barriers in $G_A(q)$ and $G_0(x)$ were found from quadratic fits to the energy profiles, as described (4).

All quantities were calculated using both unfolded-state and folded-state data. The results for measurements near $F_{½}$ are listed in Table S1 (all errors represent the standard error on the mean). The results from U and F were found to be the same within error for each quantity calculated ($\langle \delta q^2 \rangle$, τ_A, D_q, k_A, and k_M) and hence were averaged in each case to yield the values listed in Table 1.

The intrinsic molecular diffusion coefficient, D_x, was calculated from the average transition path time (τ_{tp}) obtained from constant trap position measurements, under the assumption of one-dimensional diffusive motion over a harmonic barrier in the high-barrier limit (5):

$$\tau_{tp} \approx \frac{\ln\left(2e^{\gamma}\beta\Delta G^{\ddagger}\right)}{\beta D \kappa_b}, \qquad \text{(S1)}$$

where $\Delta G^{\ddagger}$ is the barrier height in $G_0(x)$, κ_b is the barrier stiffness, γ is Euler's constant, and $\beta = 1/k_B T$ is the inverse thermal energy. Transition path times were measured directly from extension trajectories as described previously (6). Briefly, transition paths were identified as those parts of the trajectory traversing from the folded state F to the unfolded state U or vice versa. Defining the barrier region between F and U as the middle half of the distance from F to U, the transit time was measured as the time required to cross from one edge of the barrier region to the other. Transit times for all barrier crossings were averaged to obtain τ_{tp}. The diffusion coefficient D_x calculated using Eq. S1 agreed well with the value obtained from constant-force rate measurements using Kramer's equation (Table 1).

Table S1: Landscape and kinetic parameters near $F_{1/2}$

Constant force	30R50/T4		20TS06/T4	
	folded	unfolded	folded	unfolded
κ_{Aw} (k_BT/nm^2)	0.08 ± 0.01	0.09 ± 0.01	0.07 ± 0.03	0.07 ± 0.02
κ_{Ab} (k_BT/nm^2)	0.08 ± 0.01	0.08 ± 0.01	0.11 ± 0.02	0.11 ± 0.02
κ_b (k_BT/nm^2)	0.29 ± 0.03	0.29 ± 0.03	0.4 ± 0.1	0.4 ± 0.1
$\Delta G^{\ddagger}_A$ (k_BT)	4.0 ± 0.1	3.7 ± 0.2	1.9 ± 0.3	2.0 ± 0.2
$\langle \delta q^2 \rangle$ (nm^2)	11 ± 2	8 ± 2	13 ± 2	14 ± 1
τ_A (μs)	40 ± 3	36 ± 3	32 ± 2	35 ± 1
k_A (s^{-1})	110 ± 10	100 ± 10	7 ± 2 × 10^2	7 ± 1 × 10^2
k_{MA} (s^{-1})	3.3 ± 0.3	3.3 ± 0.3	11 ± 5	11 ± 4
k_M (s^{-1})	4 ± 1	4 ± 1	16 ± 4	15 ± 4
D_q (×10^5 nm^2/s)	2.6 ± 0.2	2.2 ± 0.4	4.1 ± 0.5	4.0 ± 0.4
Constant position				
κ_{AW} (k_BT/nm^2)	0.10 ± 0.02	0.12 ± 0.02	0.08 ± 0.02	0.10 ± 0.01
κ_{Ab} (k_BT/nm^2)	0.11 ± 0.02	0.11± 0.02	0.18 ± 0.03	0.18 ± 0.03
$\Delta G^{\ddagger}_A$ (k_BT)	0.80 ± 0.05	0.73 ± 0.03	0.73 ± 0.06	0.68 ± 0.06
$\langle \delta q^2 \rangle$ (nm^2)	5.2 ± 0.1	5.1 ± 0.1	5.3 ± 0.2	5.5 ± 0.3
k_A (×10^3 s^{-1})	4.1 ± 0.5	4.7 ± 0.5	6 ± 1	6 ±1
τ_A (μs)	8.5 ± 0.3	8.7 ± 0.2	9.5 ± 0.04	9.5 ± 0.3
D_q (×10^5 nm^2/s)	6.1 ± 0.5	5.9 ± 0.4	5.6 ± 0.4	5.8 ± 0.4
τ_{tp} (μs)	27 ± 2	28 ± 2	22 ± 2	23 ± 2

Table S2: Parameters for hairpin 20TS06/T4 when 99.7% unfolded.

Constant force	folded	unfolded
κ_{Aw} (k_BT/nm^2)	0.037 ± 0.006	0.033 ± 0.003
κ_{Ab} (k_BT/nm^2)	0.04 ± 0.01	0.04 ± 0.01
κ_b (k_BT/nm^2)	0.4 ± 0.1	0.4 ± 0.1
$\Delta G^{\ddagger}_A$ (k_BT)	4.3 ± 0.2	0.18 ± 0.06
$\langle \delta q^2 \rangle$ (nm^2)	14 ± 1	14 ± 1
τ_A (μs)	54 ± 2	55 ± 2
D_q (nm^2/s)	2.6 ± 0.3 × 10^5	2.7 ± 0.3 × 10^5
k_A (s^{-1})	85 ± 5	5 ± 1 × 10^3
k_{MA} (s^{-1})	1.4 ± 0.2	290 ± 20
k_M (s^{-1})	1.5 ± 0.2	330 ± 20

References

1. Woodside, M.T., W.M. Behnke-Parks, K. Larizadeh, K. Travers, D. Herschlag, and S.M. Block. 2006. Nanomechanical measurements of the sequence-dependent folding landscapes of single nucleic acid hairpins. *Proc. Natl. Acad. Sci. USA*. 103:6190–6195.

2. Neupane, K., H. Yu, D.A.N. Foster, F. Wang, and M.T. Woodside. 2011. Single-molecule force spectroscopy of the add adenine riboswitch relates folding to regulatory mechanism. *Nucleic Acids Res*. 39:7677–7687.

3. Greenleaf, W.J., M.T. Woodside, E.A. Abbondanzieri, and S.M. Block. 2005. Passive all-optical force clamp for high-resolution laser trapping. *Phys. Rev. Lett*. 95:208102.

4. Neupane, K., D.B. Ritchie, H. Yu, D.A.N. Foster, F. Wang, and M.T. Woodside. 2012. Transition path times for nucleic acid folding determined from energy-landscape analysis of single-molecule trajectories. *Phys. Rev. Lett*. 109:68102.

5. Chung, H.S., J.M. Louis, and W.A. Eaton. 2009. Experimental determination of upper bound for transition path times in protein folding from single-molecule photon-by-photon trajectories. *Proc. Natl. Acad. Sci. USA*. 106: 11837–11844.

6. Neupane, K., D.A.N. Foster, D.R. Dee, H. Yu, F. Wang, and M.T. Woodside. 2016. Direct observation of transition paths during the folding of proteins and nucleic acids. *Science*. 352: 239–242.